

Probing ion-ion and electron-ion correlations in liquid metals within the quantum hypernetted chain approximation

J. A. Anta*

Physical and Theoretical Chemistry Laboratory, Oxford University, South Parks Road, Oxford OX1 3QZ, United Kingdom

A. A. Louis

Department of Chemistry, Cambridge University, Lensfield Road, Cambridge CB2 1EW, United Kingdom

(Received 22 July 1999)

We use the quantum hypernetted chain approximation to calculate the ion-ion and electron-ion correlations for liquid metallic Li, Be, Na, Mg, Al, K, Ca, and Ga. We discuss trends in electron-ion structure factors and radial distribution functions, and also calculate the free-atom and metallic-atom form factors, focusing on how bonding effects affect the interpretation of x-ray scattering experiments, especially measurements of the ion-ion structure factor in the liquid metallic phase.

I. INTRODUCTION

Liquid metals are complex binary fluids consisting of ions in a sea of conduction electrons. While the ions can usually be treated classically, the electrons are typically degenerate and must be treated quantum mechanically. Liquids are differentiated from gases by nontrivial structure at the level of two-body correlation functions; they are generally close in density to solid phases. For two-component systems these correlation functions are defined in k space as

$$S_{\alpha\beta}(k) = \frac{\langle \hat{\rho}_\alpha(\mathbf{k}) \hat{\rho}_\beta(-\mathbf{k}) \rangle}{(N_\alpha N_\beta)^{1/2}} - (N_\alpha N_\beta)^{1/2} \delta_{k,0}. \quad (1.1)$$

The $S_{\alpha\beta}(k)$ are referred to as static structure factors and the operator

$$\hat{\rho}_\alpha(\mathbf{k}) = \sum_{i=1}^{N_\alpha} e^{i\mathbf{k} \cdot \mathbf{r}_{i\alpha}} \quad (1.2)$$

is the Fourier transform of the one-particle density operator of component α . The indices α and β refer to ions (I), or valence electrons (e). The structure factors $S_{\alpha\beta}(k)$ can be related to the so-called radial distribution functions $g_{\alpha\beta}(r)$ by

$$S_{\alpha\beta}(k) = \delta_{\alpha\beta} + (\rho_\alpha \rho_\beta)^{1/2} \int_V d\mathbf{r} e^{i\mathbf{k} \cdot \mathbf{r}} [g_{\alpha\beta}(r) - 1], \quad (1.3)$$

where the ρ_i are the homogeneous average densities.

The determination of the ion-ion structure factor $S_{II}(k)$ and the electron-electron structure factor $S_{ee}(k)$ are interesting problems in their own right (one largely quantum mechanical, the other largely classical), and have been the focus of much research: the $S_{II}(k)$ because of their experimental accessibility, the $S_{ee}(k)$ (with the ions usually smeared into a rigid neutralizing background) because of the importance of the electron fluid.¹ In contrast, the electron-ion structure factor $S_{eI}(k)$ has received considerably less attention, partially because it is hard to measure, partially because its exact physical relevance remains largely unexplored and unknown,

and partially because it includes both the physics of the ions and the physics of the electrons, each of which is traditionally treated with its own set of theoretical techniques.

One of the simplest ways to treat the valence electrons in a liquid metal is in a linear response formalism using a local pseudopotential.² In fact, linear response has been shown to be much more accurate than one would naively expect, a result which stems in part from a recently discovered interference effect between an atomic length scale, the inverse ionic length, and an electronic length scale, twice the Fermi wave vector $2k_F$.³ This interference effect significantly reduces the magnitude of the nonlinear response terms at the normal densities of most liquid metals so that electron-ion correlations emerge when the induced linear response electron density is combined with standard liquid state techniques to treat the ions.⁴⁻⁷ This approach is easy to implement, can in some cases be remarkably accurate, and can explain the qualitative trends in the shape of the electron-ion structure factor $S_{eI}(k)$ for metallic liquids across the periodic table.³ The main obstacles to higher accuracy lie in the uncertainty over the exact (local) pseudopotential, especially when nonlocal effects are important,⁸ and also in the neglect of nonlinear electron response and of ion-ion correlation effects on the induced electron densities.^{9,10}

The development of *ab initio* simulation techniques based on density-functional theory (DFT) for the electrons,¹¹ and molecular dynamics on the adiabatic electronic potential energy surface for the ions,¹² provide probably the most accurate and well-tested approach to electron-ion structure. However, the drawback of these methods is their computational cost; in practice only relatively small system sizes can be investigated and so far only results for Mg and Bi electron-ion correlations have been published.¹³ The related orbital-free *ab initio* molecular-dynamics method (OF-AIMD) (Ref. 14) allows larger system sizes and significantly longer simulation times, and has been successfully applied to the electron-ion correlations of Li, Na, Mg, and Al,^{10,15} but the computational cost is still rather large.

An alternative approach is the quantum hypernetted chain (QHNC) method of Chihara,¹⁶ which self-consistently combines integral equation techniques from the theory of simple

liquids with a Kohn-Sham-type treatment for the electrons. The QHNC treats the electrons and ions on essentially equal footing, does not require a pseudopotential approximation, and is computationally relatively cheap. Ion-ion and electron-ion correlations emerge in the thermodynamic limit—there are no finite-size effects.

In Sec. II, we use DFT to derive the basic form of the QHNC approximation by focusing first on the exact quantum Ornstein-Zernike (QOZ) equations in Sec. II A, and then outlining the approximations needed to derive the QHNC approximation in Sec. II B. The numerical implementation of the QHNC is detailed in the Appendix. Although parts of these derivations have been described in the literature before, most notably by Chihara and co-workers, including them together in a unified fashion based on DFT helps elucidate the physical meaning of the approximations made.

In Sec. III, we describe the ion-ion and electron-ion correlations that emerge from the QHNC for our set of metals: Li, Be, Na, Mg, Al, K, Ca, and Ga. Where the results are not included in the plots, they can be found in Ref. 17.

Even though the valence electron distributions are changed in a bonded environment, x-ray scattering off liquid metals has traditionally been interpreted with a free-atom form factor. In Sec. IV, we describe the difference between extracting ion-ion structure in x-ray scattering with a free-atom form factor and extracting ion-ion structure with a metallic-atom form factor. The effects of bonding on the coherent x-ray scattering intensity may be measured by comparing x-ray and neutron-scattering determinations of the ion-ion structure factor $S_{II}(k)$. However, experiments and theory have yet to converge on this issue.

Finally, we present some concluding remarks in Sec. V, and describe some details related to the numerical implementation of the QHNC in the Appendix.

II. QUANTUM HYPERNETTED CHAIN APPROXIMATION (QHNC)

A. Quantum Ornstein-Zernike relations

The quantum Ornstein-Zernike (QOZ) relations for a two-component system are most naturally derived in the context of density-functional theory (DFT).^{9,18} First we define the Helmholtz free energy for a two-component system, which is a unique functional of the two one-body density profiles:¹⁹

$$F[\rho_1, \rho_2] = F_1^{id}[\rho_1] + F_2^{id}[\rho_2] + F^{ex}[\rho_1, \rho_2]. \quad (2.1)$$

The functional is split in the usual way between ideal (non-interacting) and excess (interacting) parts. We then introduce the external potential field

$$\Psi_\alpha(\mathbf{r}) = \mu_\alpha - \phi_\alpha(\mathbf{r}), \quad (2.2)$$

which is defined in terms of the chemical potential μ_α of species α and the external potential $\phi_\alpha(\mathbf{r})$ which acts on species α only. A Legendre transform with respect to these external fields obtains the grand potential

$$\begin{aligned} \Omega[\Psi_1, \Psi_2] = & F[\rho_1, \rho_2] + \int d\mathbf{r} \rho_1(\mathbf{r}) \Psi_1(\mathbf{r}) \\ & + \int d\mathbf{r} \rho_2(\mathbf{r}) \Psi_2(\mathbf{r}), \end{aligned} \quad (2.3)$$

which is in turn a unique functional of the two external potential fields Ψ_1 and Ψ_2 .

The second functional derivative of the Helmholtz free-energy functional and the grand potential functional with respect to the relevant fields are easily obtained:

$$\frac{\delta^2 F}{\delta \rho_\alpha(\mathbf{r}) \delta \rho_\beta(\mathbf{r}')} = \frac{\delta \Psi_\alpha(\mathbf{r})}{\delta \rho_\beta(\mathbf{r}')} = \chi_{\alpha\beta}^{-1}(\mathbf{r}, \mathbf{r}'), \quad (2.4)$$

$$\frac{\delta^2 \Omega}{\delta \Psi_\alpha(\mathbf{r}) \delta \Psi_\beta(\mathbf{r}')} = \frac{\delta \rho_\alpha(\mathbf{r})}{\delta \Psi_\beta(\mathbf{r}')} = \chi_{\alpha\beta}(\mathbf{r}, \mathbf{r}'), \quad (2.5)$$

which defines the susceptibility matrix or matrix of the linear response functions $\chi_{\alpha\beta}(\mathbf{r}, \mathbf{r}')$. Thus the two second functional derivatives are each others' functional inverse, a natural consequence of having two generating functionals linked by a Legendre transform.²⁰

The direct correlation functions $C_{\alpha\beta}(\mathbf{r}, \mathbf{r}')$ of an arbitrary two-component mixture are defined in the usual way as functional derivatives of the excess free energy:²¹

$$-\frac{1}{\beta} C_{\alpha\beta}(\mathbf{r}, \mathbf{r}') = \frac{\delta^2 F^{ex}}{\delta \rho_\alpha(\mathbf{r}) \delta \rho_\beta(\mathbf{r}')}. \quad (2.6)$$

If we then define $(\chi_{\alpha\beta}^{(0)})^{-1}$ as the inverse susceptibility matrix of the ideal system, we arrive, by combining Eqs. (2.1), (2.4), and (2.6), at the following relationship between two two-by-two matrices:

$$-\frac{1}{\beta} C_{\alpha\beta} = (\chi_{\alpha\beta})^{-1} - (\chi_{\alpha\beta}^{(0)})^{-1}, \quad (2.7)$$

the QOZ relations. They follow from simple properties of the two free-energy functionals and in this form they are valid for any two-component inhomogeneous quantum system (the generalization to more than two components is straightforward). In the homogeneous limit the direct correlation functions of Eq. (2.6) reduce to the usual direct correlation functions first introduced by Ornstein and Zernike,^{22,23} and it is in this sense that we will be using them throughout the rest of this paper.

For classical species, the fluctuation-dissipation theorem relates the response functions to density-density correlation functions:²⁴

$$\lim_{\hbar \rightarrow 0} \chi_{\alpha\beta}(k, 0) = -\beta(\rho_\alpha \rho_\beta)^{1/2} S_{\alpha\beta}(k), \quad (2.8)$$

written here for a homogeneous system and in terms of the structure factors defined in Eq. (1.1). For a liquid metal, where the ions are viewed as classical but the electrons quantum mechanical, inverting the matrix in the QOZ relations of Eq. (2.7), and applying the fluctuation-dissipation theorem of Eq. (2.8) for $\chi_{II}(k)$ and $\chi_{eI}(k)$ results in

$$S_{II}(k) = [1 + \chi_{ee}^{(0)}(k) C_{ee}(k) / \beta] / D(k)$$

$$S_{eI}(k) = -\sqrt{\frac{\rho_I}{\rho_e}} \chi_{ee}^{(0)}(k) [C_{eI}(k)/\beta]/D(k) \quad g_{eI}(r) = \frac{\rho_e^0(r|v_{eI}^{\text{eff}})}{\rho_e}, \quad (2.13)$$

$$\chi_{ee}(k) = \chi_{ee}^{(0)}(k) [1 - \rho_I C_{II}(k)]/D(k)$$

$$D(k) = [1 - \rho_I C_{II}(k)] [1 + \chi_{ee}^{(0)}(k) C_{ee}(k)/\beta] + \rho_I \chi_{ee}^{(0)}(k) |C_{eI}(k)|^2/\beta, \quad (2.9)$$

where $\chi_{ee}^{(0)}(k)$ is the well-known Lindhard function,²⁵ the response function of the noninteracting electron gas. In the limit that both species are classical, the QOZ relations reduce to the usual classical two-component Ornstein-Zernike relations.²³

The QOZ relations for a liquid metal appear to have been derived by Chihara.²⁶ Later Ichimaru *et al.*²⁷ derived similar equations from a two-component linear response formulation. The two formulations are equivalent if the definitions of the direct correlation functions of Eq. (2.6) are linked in the usual way to the local-field factors $G_{\alpha\beta}(k)$:

$$\frac{C_{\alpha\beta}(k)}{\beta} = -V_{\alpha\beta}(k) [1 - G_{\alpha\beta}(k)], \quad (2.10)$$

where $V_{\alpha\beta}(k)$ is the direct potential between species.

B. Quantum hypernetted chain approximation

To solve the QOZ relations for a liquid metal we recast them into a slightly different form using two steps:⁹ The first step is to use the Percus trick²⁸ to relate the homogeneous two-body pair-correlation functions to the one-body inhomogeneous density around one particle fixed at the origin. For the electron-ion pair-correlation function we fix an ion at the origin to find

$$g_{eI}(\mathbf{0}, \mathbf{r}) = \frac{\rho_e(\mathbf{r}|I)}{\rho_e}, \quad (2.11)$$

where $\rho_e(\mathbf{r}|I)$ is the (interacting) valence electron density induced by one ion at the origin. A similar relationship holds for the ion-ion pair-correlation function, but for the electron-electron pair correlation function the Percus trick cannot be used in this form; one cannot ‘‘fix’’ an electron at the origin.

The second step follows the basic ideas of the Kohn-Sham scheme,¹¹ namely that there exists a local single-particle external potential $v^{\text{eff}}(\mathbf{r})$ which will induce in a noninteracting system the same one-particle density $\rho(\mathbf{r})$ as is found in the full interacting system. This idea holds both for quantum as well as for classical systems. The external effective potential felt by species α when species β is fixed at the origin follows directly from the Euler equations:

$$v_{\alpha\beta}^{\text{eff}}(r) = v_{\alpha\beta}(r) + \frac{\delta F^{\text{ex}}}{\delta \rho_{\alpha}(\mathbf{r})} - \mu_{\alpha}^{\text{ex}}, \quad (2.12)$$

where $v_{\alpha\beta}(r)$ is the direct interaction between species and μ_{α}^{ex} is the excess chemical potential. Thus the electron-ion radial distribution function follows from the indirect Kohn-Sham solution of the Euler-equation combined with the Percus identity:

where $\rho_e^0(r|v_{eI}^{\text{eff}})$ is the density of the unbound (or free) valence electrons obtained from the wave functions that emerge from a Kohn-Sham solution of the one-center radially symmetric noninteracting Schrödinger equation in the external effective potential given by Eq. (2.12).¹¹ The ion-ion radial distribution function follows from a direct solution of the ion-ion Euler equation combined with the Percus identity:

$$g_{II}(r) = \frac{\rho_I(r|I)}{\rho_I} = \frac{\rho_I^0(r|v_{II}^{\text{eff}})}{\rho_I} = \exp[-\beta v_{II}^{\text{eff}}(r)], \quad (2.14)$$

where in the classical context $v_{II}^{\text{eff}}(r)$ is commonly referred to as the potential of mean force. Next we expand the effective potentials $v_{II}^{\text{eff}}(r)$ and $v_{eI}^{\text{eff}}(r)$ in a functional Taylor expansion around the equilibrium homogeneous densities and rewrite Eq. (2.12) as

$$v_{\alpha I}^{\text{eff}}(r) = v_{\alpha I}(r) - \frac{1}{\beta} \sum_{\gamma} \rho_{\gamma} \int C_{\alpha\gamma}(|\mathbf{r}-\mathbf{r}'|) h_{\gamma I}(r) d\mathbf{r}' + \frac{1}{\beta} B_{\alpha I}(r), \quad (2.15)$$

where the $C_{\alpha\gamma}(r)$ are the homogeneous limits of Eq. (2.6), and the Percus trick was used to rewrite $[\rho_{\gamma}(\mathbf{r}|v_{\gamma I}) - \rho_{\gamma}]$ in terms of the correlation functions $h_{\gamma I}(r) = g_{\gamma I}(r) - 1$. The remaining third and higher-order functional derivative terms are lumped into the so-called bridge functions $B_{\alpha\beta}(r)$. We note that these equations do not hold for the effective electron-electron potential $v_{ee}(r)$.

Up to this point, our formulation is in principle exact. However, since the exact free-energy functionals and the related effective external potentials are unknown, some approximations must be made. In the language of the theory of classical liquids,²³ we need a closure relation. For this we follow the approach developed by Chihara, which he named the quantum hypernetted chain approximation (QHNC).¹⁶ The main approximations made by Chihara are (roughly in ascending order of importance)

(i) The bare ion-ion potential is taken to be purely Coulombic. This neglects core polarization effects, but these are expected to be small in the metals we study.

(ii) The ion-ion bridge function $B_{II}(r)$ is approximated by the one-component bridge function of an appropriate reference state. This is commonly called the RHNC or MHNC approximation,²⁹ and is expected to be quite accurate. We use the repulsive part of the one-component effective pair potential solved in the Percus-Yevick approximation as a reference system to calculate the bridge function (see the Appendix for details).

(iii) The electron-ion bridge function $B_{eI}(r)$ is set to 0. This is commonly called the hypernetted chain (HNC) approximation, and is generally also quite accurate, especially as the electron-ion correlations are expected to be weaker than the ion-ion correlations.

(iv) The local density approximation (LDA) is used for the one-center electron-ion problem. The calculation of the

electron-ion correlation function reduces to calculating the Schrödinger equation in the external potential given by Eq. (2.15). This is similar to a self-consistent field all-electron calculation for a single atom, except that the potential includes not only the nuclear Coulomb contribution, but also terms reflecting the effect of the surrounding ions. We solve this effective atomic problem in the LDA, which is widely used in electronic structure calculations. The core electrons are treated explicitly, i.e., this is an all-electron calculation. However, the core and valence screening effects are separated in a manner similar to the linear unscreening procedure used to derive pseudopotentials.³⁰

(v) The valence electron correlations are treated in the jellium approximation. To calculate the full effective potentials, we need the electron-electron direct correlation function $C_{ee}(k)$, which can be rewritten in terms of the so-called local-field factors as was done in Eq. (2.10) where the non-Coulombic correlation part has been subsumed into the local-field factor $G(k)$. In the QHNC approach, the local-field factor is approximated to be that of jellium at the average electron density, i.e., it is independent of ionic correlations:

$$C_{ee}(k) = -\beta v_{ee}(k)[1 - G_{ee}^{jell}(k; \rho_e)]. \quad (2.16)$$

Thus the electron-electron direct-correlation function uncouples from the other correlation functions in Eq. (2.9). This approximation is similar in spirit to the LDA approximation and greatly simplifies part of the electronic problem, but it is probably the most serious and uncontrolled part of the QHNC closure.

The approximations for the bridge functions together with Eqs. (2.13), (2.14), (2.15), and the closure for $C_{ee}(k)$ in Eq. (2.16) reduce the QOZ relations of Eq. (2.9) to a closed pair of coupled equations for the radial distribution functions:

$$\begin{aligned} \rho_e g_{ei}(r) = & \rho_e \left(r |v_{ei}(r) - \frac{1}{\beta} \rho_I \int C_{ei}(|\mathbf{r}-\mathbf{r}'|) h_{II}(r) d\mathbf{r}' \right. \\ & \left. - \frac{1}{\beta} \rho_e \int C_{ee}(|\mathbf{r}-\mathbf{r}'|) h_{ei}(r) d\mathbf{r}' \right), \quad (2.17) \end{aligned}$$

$$\begin{aligned} g_{II}(r) = & \exp \left(-\beta v_{II}(r) + \rho_I \int C_{II}(|\mathbf{r}-\mathbf{r}'|) h_{II}(r) d\mathbf{r}' \right. \\ & \left. + \rho_e \int C_{Ie}(|\mathbf{r}-\mathbf{r}'|) h_{ei}(r) d\mathbf{r}' - \frac{1}{\beta} B_{II}(r) \right) \quad (2.18) \end{aligned}$$

which are solved self-consistently. This is the essence of the QHNC approach: the original many-center problem has been reduced to an effective one-center problem by replacing the many-body ion-ion correlations with an effective external potential that depends self-consistently on the ion-ion correlations. The main advantages are that (a) no pseudo-potential is needed, i.e., it is an all-electron calculation and (b) ion-ion and electron-ion correlations emerge naturally and on the same footing. Details of the (rather complex) numerical implementation of the QHNC are described in the Appendix.

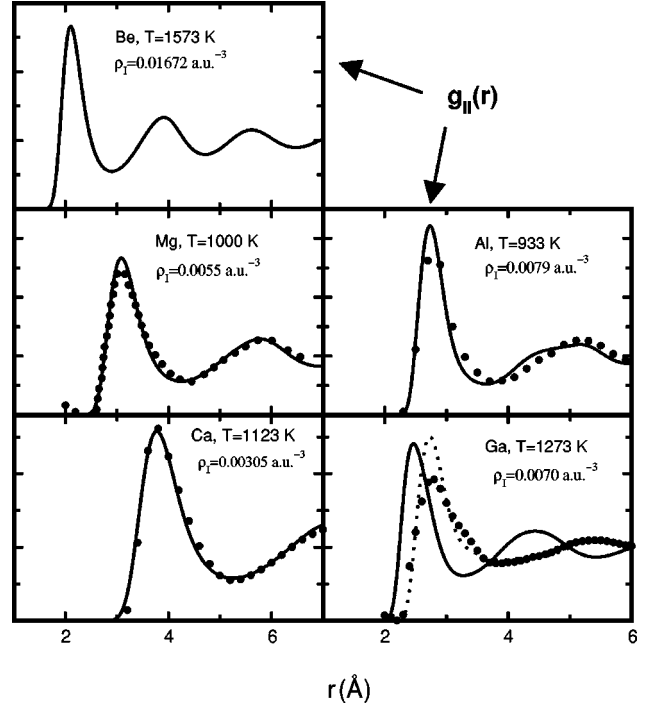


FIG. 1. Ion-ion radial distribution functions $g_{II}(r)$ calculated by means of the QHNC method (solid lines) and compared to x-ray experiments (circles) (Ref. 31). The dotted lines in the Ga panel correspond to QHNC with the Ortiz-Ballone $G(q)$ (Ref. 32). Results for the other metals in our set can be found in Ref. 17.

III. ION-ION AND ELECTRON-ION CORRELATIONS

A. Ion-ion radial distribution function

Armed with the QHNC approach, we can now tackle the electron-ion and ion-ion correlation functions for a set of simple metals from the first four rows of the periodic table. As a test of the approach, we compare in Fig. 1 the QHNC ion-ion radial distribution function for part of our set of metals to the experimental x-ray data of the Waseda group.³¹ The QHNC provides a faithful representation of $g_{II}(r)$ for all the metals except Ga. The accuracy of the QHNC for the other elements suggests that it can also be trusted for Be, for which no experimental data could be found. Our results are the same as those of J. Chihara and co-workers for the metals they studied.

The case of Ga, however, calls for closer examination. While the exact form of $g_{II}(r)$ is sensitive to details of the liquid state theory aspects of the closure, i.e., the form of the bridge function, we tried various forms of the closure without much improvement. On the other hand, when we used the Ortiz-Ballone³² local-field factor instead of the Ichimaru-Utsumi form,³³ a considerable improvement was obtained, in agreement with earlier studies based on effective ion-ion potentials.⁵ This sensitivity of the QHNC approach to details of the local-field factor $G(q)$ suggests that approximation (v) of the previous section begins to break down. In addition, the d electrons were very close to being unbound, which made the QHNC algorithm difficult to converge. This instability may be attributed to the implicit separation of the exchange-correlation potential into bound and valence contributions in approximation (iv), i.e., the neglect of nonlinear-core corrections. The fact that the Ortiz-Ballone $G(q)$ seems to work

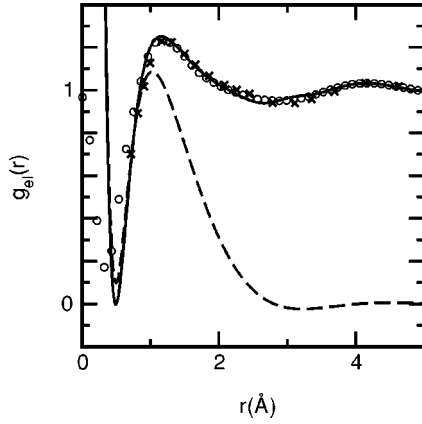


FIG. 2. Electron-ion radial distribution function of Mg as obtained from the QHNC approximation (solid lines), the Orbital-free method (Ref. 10) (open circles) and Car-Parrinello molecular dynamics (Ref. 13) (crosses). The dashed lines represent the pseudoatom density $n(r)/\rho_e$. Results for the other metals in our set can be found in Ref. 17.

better for Ga is most likely due to an accidental cancellation of errors. It performs considerably worse than the LDA or Ichimaru-Utsumi $G(q)$ (Ref. 33) for the other metals in our set.

B. Pseudoatoms and electron-ion correlations

The electron-ion structure factor, defined by Eq. (1.1), can always be rewritten in the following fashion:

$$S_{eI}(k) = \frac{n(k)}{\sqrt{Z}} S_{II}(k), \quad (3.1)$$

which defines a new object $n(k)$. By taking the Fourier transform we find, using Eq. (1.3), the electron-ion radial-distribution function:

$$\rho_e g_{eI}(r) = n(r) + \rho_i^0 \int_V n(|\mathbf{r} - \mathbf{r}'|) g_{II}(r') d\mathbf{r}', \quad (3.2)$$

which is proportional to the probability of finding an electron a distance r away from an ion located at the origin. Thus a natural interpretation of $n(r)$ is the density of a ‘‘pseudoatom,’’ which, when superimposed according the ion-ion radial-distribution function $g_{II}(r)$ gives the correct value of the valence electron distribution. The pseudoatom is independent of ionic correlations only to first order in the electron-ion potential, at higher orders it implicitly includes three-body and higher-order ionic averages.^{3,8,9}

In the QHNC approximation, the electron-ion radial-distribution function follows directly from the solution of the one-body Schrödinger equation [Eq. (2.13)]. In Fig. 2 we show the electron-ion radial-distribution functions $g_{eI}(r)$ for our set of metals. Where possible, they have been compared to *ab initio* Kohn-Sham¹³ and OF-AIMD (Ref. 10) results. As is the case for the ion-ion radial distribution functions, the QHNC approximation gives similar results to other methods for all the elements except Ga, where once again an improved agreement is obtained when the Ortiz-Ballone $G(q)$ is used.

It is instructive to compare the pseudo-atom density, included in Fig. 2 as $n(r)/\rho_e$, with the electron-ion radial distribution function $g_{eI}(r)$. The pseudoatom density goes to zero for larger r , as it is essentially localized around a given ion, while $g_{eI}(r)$ goes to 1 for large r , reflecting the fact that outside the range of the ion’s own pseudoatom, $g_{eI}(r)$ simply probes the average density of the pseudoatoms around the other ions so that the probability of finding a valence electron a distance r away is simply related to the probability of finding an ion there. $g_{eI}(r)$ and $n(r)/\rho_e$ are essentially identical for small r , as one might expect, while at larger r the effect of the ion-ion weighted superposition of the surrounding pseudoatoms on $g_{eI}(r)$ is evident. Because $g_{eI}(r)$ implicitly includes a spherical average, all angular bonding effects are effectively washed out, although an indication of the effect of bonding can still be found by comparing $g_{eI}(r)$ and a superposition of the free-atom electron densities.¹³

The relationships between the pseudoatom, the ionic correlations, and the electron-ion correlations become clearer in k space where the electron ion structure factor is simply the product of the pseudoatom density and the ion-ion structure factor, as shown in Eq. (3.1). The ion-ion structure factor is sharply peaked at its first maximum k_p while the pseudoatom density goes through zero at \bar{k}_0 . If $\bar{k}_0 < k_p$, the product form implies that the first peak of $S_{eI}(k)$ is negative, and the electron-ion structure is in the so-called low valence class, while if $\bar{k}_0 > k_p$, then the first peak of $S_{eI}(k)$ is positive, and the electron-ion structure is in the so-called high valence class.^{3,9} In Fig. 3 we plot both the electron-ion structure factors $S_{eI}(k)$ and the pseudoatom densities $n(k)$ for our set of metals. Li, Be, Na, Mg, and K are in the low valence class, while Al and Ga straddle the two classes. Only Ca seems to fall outside this taxonomy.

IV. USING FREE-ATOM FORM FACTORS VS METALLIC-ATOM FORM FACTORS

Neutron scattering probes the fluctuations of the nuclei, while x-ray scattering probes the fluctuations of all the electrons. In 1974, Egelstaff *et al.*³⁴ suggested exploiting this difference to extract electron-ion correlations for liquid metals. In 1987, Chihara³⁵ re-examined the x-ray scattering problem, demonstrating that a careful analysis of elastic and inelastic contributions leads to the following coherent scattering intensity:¹⁰

$$I_X(k) = |f_I(k) + n(k)|^2 S_N(k), \quad (4.1)$$

where $S_N(k)$ is the nucleus-nucleus structure factor which emerges, for example, from neutron scattering, $f_I(k)$ is the ionic form factor, i.e., the ionic electron density, and $n(k)$ is the pseudoatom density. We shall call the object $f_M(k) = f_I(k) + n(k)$ the metallic-atom form factor. Traditionally the structure factor from x-ray scattering $S_X(k)$ has been extracted from scattering intensity as follows:

$$I_X(k) = |f_A(k)|^2 S_X(k), \quad (4.2)$$

where $f_A(k)$ is the free-atom form factor, or the free-atom electron density.

The difference between the two structure factors $S_N(k)$ and $S_X(k)$ stems from the difference between the two form

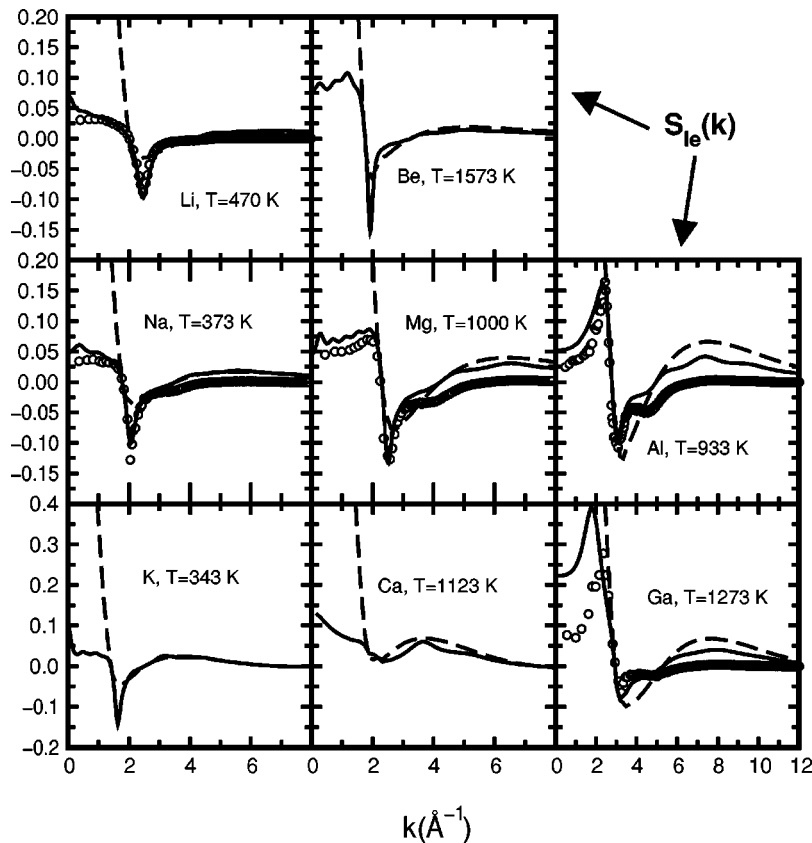


FIG. 3. Electron-ion structure factors $S_{el}(k)$. The symbols have the same meaning as in Fig. 2, the dashed lines again represent the pseudoatom density $n(k)$, but now in k space. For the scale, note that $n(k=0)=Z$, the number of valence electrons.

factors $f_A(k)$ and $f_M(k)=f_I(k)+n(k)$, and provides a measure of the change in electron density upon bonding. In Fig. 4 we plot the full free-atom (solid lines), metallic (dashed lines), and ionic (dotted lines) form factors for our set of metals. Also included are the pseudoatom densities (chain lines). The ionic form factor is essentially the same in the metallic and the free-atom environments, so the difference between the metallic and free-atom form factors stems from the difference between the pseudoatom density and the valence-electron density of the free atom.

Because x-rays scatter off all the electrons, not just the valence electrons, the effects of bonding are most pronounced when the ratio of the number of valence electrons Z to the total number of electrons Z_A is high. Thus, as can be seen in Fig. 4, the effects are largest in Li and Be, where the ratios ($Z:Z_A$) are (1:3) and (1:2), respectively, and the effect becomes smaller for the other elements, where the ratios are Na: (1:11), Mg: (1:6), Al:(1:4.3), K: (1:19), Ca: (1:10), and Ga:(1:10.3).

In crystalline systems, x-ray studies of charge densities only provide information on the bonding density for certain fixed scattering peaks. Similarly, in liquids the scattering is strongest at the first peak of the structure factor (at wave number k_p), so to observe a difference between $S_X(k)$ and $S_N(k)$ it is important that the free-atom and the metallic-atom form factors differ near k_p . This is demonstrated for Be in Fig. 5. Even though the difference between the free-atom and metallic-atom form factors is largest at k 's less than k_p , the experimentally accessible difference, $S_X(k) - S_N(k)$, is largest at k_p .

In Fig. 6 the difference, $S_X(k) - S_N(k)$, is shown for our whole set of metals. Generally the peak height for $S_X(k)$ is

slightly lower than the peak height for $S_N(k)$ and the two structure factors are virtually identical away from k_p . As was anticipated in Ref. 3, the largest difference is for Be, where $S_X(k_p)$ is about 5% lower than $S_N(k_p)$. However, Be is extremely toxic, and for that reason its static structure has not yet been measured. Perhaps the best chance of observing a difference between $S_X(k)$ and $S_N(k)$ is for Li, Mg, or Al, where the difference at k_p is about 2%. Another possibility includes liquid metallic Si, where the ratio is (1:3.5), and \bar{k}_0 is expected to be greater than k_p (i.e., Si's electron-ion structure is expected to be in the high valence class), so that $S_X(k_p)$ is expected to be larger than $S_N(k_p)$ and the structure factor may peak in a region where the two form factors differ by a larger amount than is the case for the low valence class metals.

Measuring these differences will be extremely challenging, since they require two completely different scattering techniques, which implies subtracting two different sets of systematic corrections. In particular, the removal of incoherent scattering effects from the total scattering remains under discussion.^{36,35,37} We note that a series of experiments measuring the differences between x-ray and neutron-scattering determinations of $S_{II}(k)$ have been reported for Li,³⁶ Na, Mg, Al, Zn, Ga, Sn, Te, Tl, Pb, and Bi.³⁸ Except for the case of Li, these measurements typically show differences that are at best five to ten times larger than expected from theoretical treatments of the bonding effects, such as those shown for the QHNC in Fig. 6.¹⁰ In fact, for some of the heavier elements, where the $S_X(k) - S_N(k)$ is expected to be very small due to the large number of core electrons, the differences are several orders of magnitude larger. In Fig. 6, we include explicitly the combined x-ray and neutron data of Olbrich

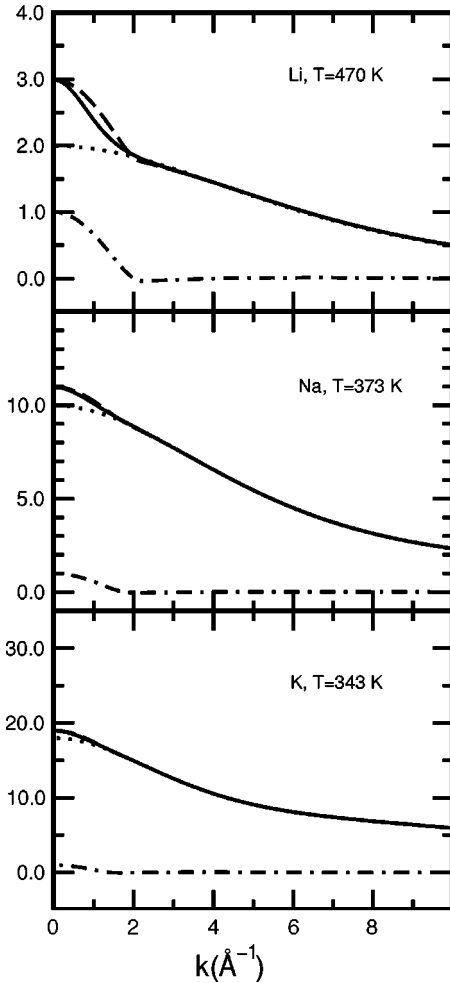


FIG. 4. Free-atom form factors $f_A(k)$ (solid lines), metallic-atom form factors $f_M(k) = f_I(k) + n(k)$ (dashed lines), and ionic form factors $f_I(k)$ (dotted lines), as predicted by the QHNC theory. The chain lines represent the pseudoatom density $n(k)$. Results for the other metals in our set can be found in Ref. 17.

*et al.*³⁶ for Li. Even though their differences are smaller than any of the differences measured in the other references cited in Ref. 38 (in fact, they are the only measurements which fit within the scale of our graphs,¹⁰) Olbrich *et al.*³⁶ claim that experimental errors are too large to see bonding effects in $S_{II}(k)$. For these reasons, the interpretation of the measurements in Ref. 38 has been called into question by a number of authors.^{44,39,5,10,3,15} The theoretical results are very robust, with simple linear response theories in some cases agreeing quantitatively with the much more sophisticated *ab initio* Kohn-Sham calculations.³ In a crystalline environment, the Kohn-Sham approach has been shown to agree quantitatively to several significant figures with highly accurate experimental measurements of the bonding densities,⁴⁰ suggesting that the electron densities calculated within the Kohn-Sham approach for the liquid state analogon of these solid state measurements should be highly accurate as well. In fact, for the Kohn-Sham-type simulations, finite size and statistical finite simulation time effects on the ion-ion structure probably cause larger errors than errors arising from the determination of the electron densities. However, these simulation errors are well understood, and will at most contribute a few relative percent to the difference $S_X(k) - S_N(k)$. The consider-

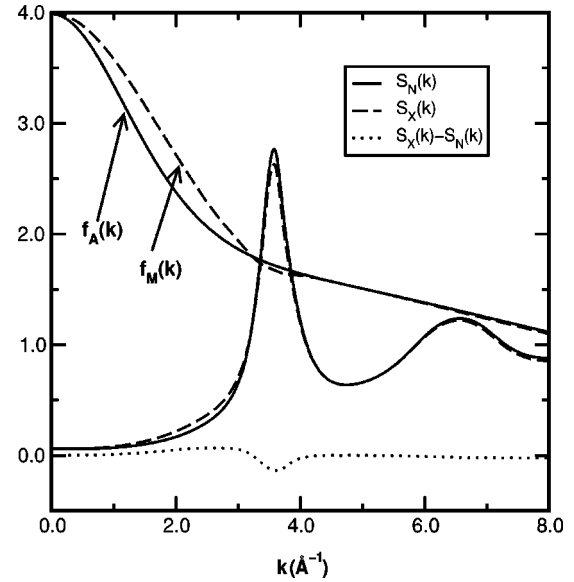


FIG. 5. The structure factors $S_N(k)$ (solid line) and $S_X(k)$ (dashed line), of liquid Be. The dotted line corresponds to the difference $S_X(k) - S_N(k)$. The metallic-atom and the free-atom form factor of Li are also included in the figure. Similar results for Li can be found in Ref. 17.

ations above, coupled with the difficulties in dealing with the subtraction of two very different sets of systematic corrections to the data,⁴¹ lead us to conclude that the experiments cited have not yet attained an accuracy sufficient to measure the effects of bonding in liquid metals.

However, the advent of new high-accuracy x-ray and neutron beam sources coming on line, together with the improvement of other techniques such as anomalous x-ray scattering,⁴² may bring the measurement of these differences within experimental reach, at least for a few of the metals in our set. It seems increasingly unlikely that this could be measured for many other elements where the ratio Z/Z_A is smaller and the core electrons wash out any bonding effects.

V. CONCLUDING REMARKS

We have carried out QHNC calculations for Li, Be, Na, Mg, Al, K, Ca, and Ga. The QHNC formalism, introduced and mainly developed by Chihara^{26,16,43,44} is a closure to the QOZ relations, which are easily derived in the context of DFT. Ion-ion and electron-ion correlations naturally emerge in a unified fashion, and the interpretation of liquid metals in terms of a “pseudoatom” helps clarify the meaning of the electron-ion radial distribution functions and structure factors.

The most serious approximation in the QHNC is probably approximation (v) from Sec. II B, where the electron-electron direct-correlation function $C_{ee}(k)$ is approximated by the jellium form, making it independent of the ion-ion and electron-ion correlations. The sensitivity to the local-field factor $G_{ee}(k)$ found for Ga may stem from a breakdown of approximation (v), but also from the neglect of nonlinear-core corrections implicit in approximation (iv). Future work will address both these issues.

The QHNC reduces to a linear-response formalism if the direct-correlation function $C_{ei}(r)/\beta$ is approximated by its

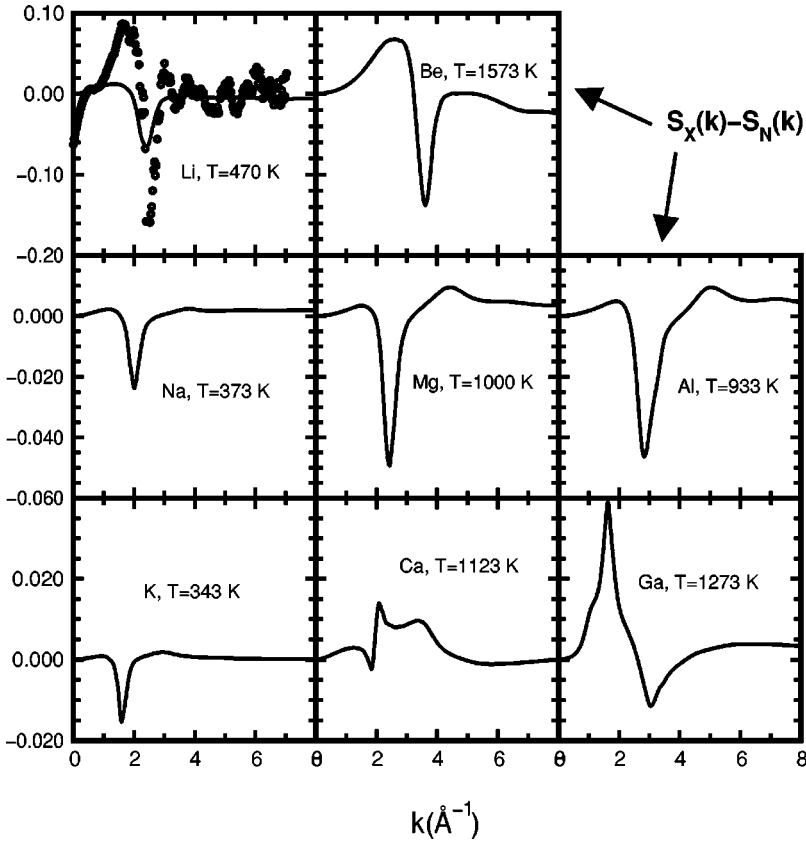


FIG. 6. Differences between using a free-atom and a metallic-atom form factor to interpret x-ray scattering determinations of the static structure factor $S_{II}(k)$ for a number of systems as predicted by the QHNC theory (note the change in scale from panel to panel). Alternatively, this can be viewed as the difference between x-ray and neutron-diffraction determinations of the ion-ion structure factor. Also included are the experimental differences between x-ray and neutron diffraction for the ion-ion structure factors of Li from Ref. 36.

low-density or long-range form $-v_{eI}(r)$, suggesting that the accuracy of the QHNC probably benefits from an interference effect which reduces the nonlinear response terms.^{9,3} For metallic hydrogen, where the lack of core electrons implies no interference effect, $C_{eI}(r)/\beta$ will differ significantly from its low-density limit. The relative importance of nonlinear response terms also suggests that approximation (v) may be poor for H. In addition, Xu *et al.*⁴⁵ showed that small changes in $C_{eI}(r)/\beta$ can have a large effect when input into DFT theories of the freezing of monatomic H. We expect the DFT theories to be relatively less sensitive to changes in $C_{eI}(r)/\beta$ when applied to the simple metals in our set.

The differences between x-ray measurements of the ion-ion structure factor $S_{II}(k)$ interpreted with a free-atom or with a metallic-atom form factor are the main experimentally relevant quantities we calculate. This difference, which reflects the effects of metallic bonding of the valence electrons, is largest for elements with a large ratio of valence to core electrons, such as Li, Be, Mg, Al, and maybe Si. To date these bonding effects have not been convincingly observed, but with new higher precision instruments coming on line, they may soon be experimentally accessible.

ACKNOWLEDGMENTS

We thank P. A. Madden, L. E. González, P. Salmon, D. L. Price, and M. L. Saboungi for helpful discussions, D. Rowan for a critical reading of the manuscript, and J. Chihara for help with some details of the implementation. A.A.L. thanks N. W. Ashcroft for his insight in early stages of this work, and P. A. Madden for hospitality at Oxford, where some of this work was completed. A.A.L. also thanks the EEC for support through Grant No. EBRFMBICT972464. J.A.A.

thanks Ministerio de Educación y Cultura of Spain for financial support in Oxford.

APPENDIX: PRACTICAL IMPLEMENTATION OF THE QHNC APPROXIMATION

1. Overview of the implementation

In the practical implementation, we follow two steps to self-consistency.

Step 1: the ion-ion loop. For a given $g_{eI}(r)$ and $C_{eI}(r)$, an effective one-component ion-ion effective potential is calculated and the one-component RHNC integral equation is solved self-consistently for $g_{II}(r)$.

Step 2: the electron-ion loop. For a given $g_{II}(r)$ and the old $g_{eI}(r)$ and $C_{eI}(r)$, an effective electron-ion potential $v_{eI}^{\text{eff}}(r)$ is calculated from Eq. (2.15). The self-consistent Schrödinger equation is then solved to give a new $g_{eI}(r)$ via Eq. (2.13), and the procedure is repeated to obtain self-consistency in $g_{eI}(r)$. These two steps are then repeated until full self-consistency is obtained between the two loops.

2. Details of the the ion-ion loop

We first rewrite the ion-ion problem as an effective one-component system with the same radial distribution function:

$$g_{II}(r) = \exp[v_{II}^{\text{eff}}(r)] = g(r) = \exp[v_1^{\text{eff}}(r)], \quad (\text{A1})$$

where $v_{II}^{\text{eff}}(r)$ is the effective potential of mean force for the ions, given by Eq. (2.15), and $v_1^{\text{eff}}(r)$ is the effective potential of mean force for the one-component system. The equality of the two radial-distribution functions then implies that

$$\begin{aligned} & -\beta v_{II}(r) + h_{II}(r) - C_{II}(r) + B_{II}(r) \\ & = -\beta v_1(r) + h(r) - C(r) + B(r), \end{aligned} \quad (\text{A2})$$

where $v_1(r)$ is the bare potential of the effective one-component system, $C(r)$ is its direct correlation function, and $B_{II}(r)$ and $B(r)$ are the bridge functions of the two-component and effective one-component systems, respectively. We follow Chihara and make the approximation⁴⁶

$$B_{II}(r) \approx B(r), \quad (\text{A3})$$

which, together with the QOZ relations of Eq. (2.9), implies that

$$v_1(r) = v_{II}(r) - \frac{\chi_{ee}^{(0)}(k) |C_{eI}(k)/\beta|^2}{1 + \chi_{ee}^{(0)}(k) C_{ee}(k)/\beta}. \quad (\text{A4})$$

Note that if the electron-ion direct correlation function is replaced by its low density or long-range limit, $C_{eI}(r)/\beta = -v_{eI}(r)$, and Eq. (2.16) is used for $C_{ee}(k)$, the effective one-component potential reduces to the usual linear screening form.²

Having now reduced the problem to an effective one-component form [by assuming a fixed $g_{eI}(r)$ and $C_{eI}(r)$], we solve the self-consistent RHNC equations in the usual way.^{23,47,48} The bridge function is obtained using as a reference system the repulsive part of the $v_1(r)$ solved in the Percus-Yevick approximation⁴⁹ which is known to perform well for short-range potentials.²³ The bridge function obtained in this way gives very similar results to the standard RHNC approximation (where the reference system is the hard-sphere fluid) for the systems here studied but with the advantage that no optimization of the hard-sphere diameter is required. This feature is specially recommended in the context of the QHNC theory, where the RHNC equation is solved in combination with the ion-electron integral equation.

3. Details of the electron-ion loop

For a given $g_{II}(r) = g(r)$, and an old $g_{eI}(r)$ and $C_{eI}(r)$, the new effective electron-ion potential follows from Eq. (2.15):

$$\begin{aligned} v_{eI}^{\text{eff}}(r) &= v_{eI}(r) - \rho_e \int \frac{C_{ee}(|\mathbf{r}-\mathbf{r}'|)}{\beta} h_{eI}(r) d\mathbf{r}' \\ & - \rho_I \int \frac{C_{eI}(|\mathbf{r}-\mathbf{r}'|)}{\beta} h_{II}(r) d\mathbf{r}', \end{aligned} \quad (\text{A5})$$

where the first term $v_{eI}(r)$ is the bare electron-ion interaction, the second term describes the screening by the valence electrons, both those of the central ion as well as those originating from the pseudoatom densities of the surrounding ions, and the third term describes the interaction of the electrons with the other ions. For the local-field factors implicit in $C_{ee}(k)$, we used the Ichimaru-Utsumi form,³³ but except for Ga, the simpler LDA form also performed quite well. For the bare electron-ion interaction we follow Chihara⁴³ and write

$$\begin{aligned} v_{eI}(r) &= -\frac{Z_A e^2}{r} + \int v_{ee}(|\mathbf{r}-\mathbf{r}'|) \rho_e^b(r) d\mathbf{r}' \\ & + \mu_{XC}[\rho_e^b(r) + \rho_e] - \mu_{XC}[\rho_e], \end{aligned} \quad (\text{A6})$$

where Z_A is the nuclear charge, $\mu_{XC}[\rho(r)]$ is the exchange-correlation part of the free energy functional (we take the usual LDA parameterization of Perdew and Zunger⁵⁰ of the Ceperley-Alder quantum Monte Carlo simulations⁵¹), and $\rho_e^b(r)$ is the bound electron density obtained from the solution of the Schrödinger equation. This form is not exact within the LDA, as its derivation implies a linear unscreening process, neglecting the so-called nonlinear-core corrections.³⁰ In fact, this linear unscreening process is not necessary, and the full screening from the combined valence and core electron densities can be taken into account, but this will be addressed in a later publication.

Using this effective electron-ion potential, the one-electron Schrödinger equation,

$$\left[-\frac{\hbar^2}{2m_e} \nabla^2 + v_{eI}^{\text{eff}}(r) \right] \psi_e^i(r) = \epsilon_e^i \psi_e^i(r), \quad (\text{A7})$$

is solved for the effective potential of Eq. (A5). The bound electron density is then calculated by means of

$$\rho_e^b(r | v_{eI}^{\text{eff}}) = \rho_e^b(r) = \sum_{i(b)} |\psi_e^{i(b)}(r)|^2, \quad (\text{A8})$$

where the index (b) refers to bound states, while $\rho_e^f(r)$, the unbound density directly related to $g_{eI}(r)$ through Eq. (2.13) corresponds to the continuum part of the eigenvalue spectrum (positive energies) and is calculated as a superposition of scattering states. In atomic units this is given by^{52,53}

$$\rho_e^f(r | v_{eI}^{\text{eff}}) = \rho_e + \frac{1}{\pi^2} \int_0^{k_F} dk k^2 \sum_l (2l+1) [R_{kl}^2(r) - j_l^2(rk)], \quad (\text{A9})$$

where k_F is the Fermi wave vector and $R_{kl}(r)$, the radial part of the wave function, is a solution of the equation

$$\frac{d^2(rR_{kl})}{dr^2} + \left[k^2 - \frac{l(l+1)}{r^2} - 2v_{eI}^{\text{eff}}(r) \right] rR_{kl}(r) = 0. \quad (\text{A10})$$

$R_{kl}(r)$ must be normalized by its asymptotic limit, i.e.,

$$\lim_{r \rightarrow \infty} [rR_{kl}(r)] = j_l(rk) \cos \eta_l(k) + n_l(rk) \sin \eta_l(k), \quad (\text{A11})$$

where $j_l(x)$ and $n_l(x)$ are spherical Bessel functions and $\eta_l(k)$ is the phase shift. The phase shifts at the Fermi level fulfill the Friedel sum rule:⁴³

$$\frac{2}{\pi} \sum_l (2l+1) \eta_l(k_F) = Z S_{II}(0), \quad (\text{A12})$$

where Z is the ionic charge and $S_{II}(0)$ the long-wavelength limit of the ion-ion structure factor.

We solve the Schrödinger equation in two stages:

(i) We first look for bound states and the eigenvalues of Eq. (A7) using the predictor-corrector method on a logarithmic grid.⁵⁴

(ii) Once the bound density is computed [needed to obtain the electron-ion bare interaction via Eq. (A6)], we solve Eq. (A10) for scattering states on a Hermann-Skillmann mesh using the Numerov method. Both the logarithmic and the Hermann-Skillmann grids, as well as the linear mesh in which the correlation functions are stored, span the same range of 40.96 a.u. (see below for numerical details). We follow Chihara and introduce a cutoff radius r_{cut} outside which the solutions are taken to be of the usual Friedel oscillatory form:

$$v_I(r) \propto \frac{1}{4\pi r^3} \cos(2k_F r), \quad r > r_{\text{cut}}, \quad (\text{A13})$$

where r_{cut} is typically equal to around 4–5 times the electron Wigner-Seitz radius. This procedure avoids difficulties with the long-range nature of the potentials while keeping the number of mesh points needed at a manageable level. Typically, we needed four or five iterations of the ion-ion and electron-ion loops for a maximum tolerance of 0.1% error between successive solutions to converge. The screening relation

$$\int \rho_e^f(r) d\mathbf{r} = Z \quad (\text{A14})$$

is fulfilled with an error around 0.1% for the lower valence metals, and less than 1% for Ga or Al. Although this is somewhat unsatisfactory, and is a larger error than that reported in previous studies,^{52,53} we found that it does not affect the shape of the correlation functions or the effective pair potential at short and intermediate distances. Future work will address this issue in more detail.

We use a linear grid of 4096 points for the ion-ion and electron-ion correlation functions (i.e., a grid size of 0.01 a.u. for a maximum distance of 40.96 a.u.). The logarithmic grid contains 983 points whereas the Hermann-Skillmann grid comprises five blocks of typically 80, 40, 40, 90, and 800 points, respectively. This corresponds to a grid size of

0.0015 a.u. for the first block. The Schrödinger equation for scattering states is solved for 25 equally spaced k points between 0 and k_F and up to 11 plane waves ($l_{\text{max}} = 10$). Then, the integral in Eq. (A9) is computed using Simpson's rule with the same number of k points. An interpolation by cubic splines is employed to swap between the different grids involved in the calculation (linear for correlation functions and logarithmic and Hermann-Skillmann grids to solve the Schrödinger equation). Fast Fourier transforms are used to convert correlation functions from real to reciprocal space. In addition, we have implemented Ng's method⁵⁵ in the ion-ion and the ion-electron loops to accelerate the convergence.

4. Details of the initial setup

As mentioned before, the implementation of this iterative procedure requires an initial effective pair potential. Following Chihara,⁴⁴ we make use of the so-called jellium-vacancy model (JVM) to obtain such initial potential. The JVM can be derived directly from the QHNC approach by the following two approximations:

(i) The ion-ion correlation function approximated as a step function,

$$h_{II}(r) = \begin{cases} -1 & \text{for } r < R, \\ 0 & \text{for } r > R, \end{cases} \quad (\text{A15})$$

where R is the ion Wigner-Seitz radius, i.e., $R = [3/(4\pi\rho_I)]^{1/3}$.

(ii) The electron-ion DCF used in the effective electron-ion interaction of Eq. (A5) is approximated to be of a purely Coulombic form,

$$C_{eI}(r)/\beta = \frac{Z_I e^2}{r}. \quad (\text{A16})$$

These two approximations result in an electron-ion potential $v_{eI}^{\text{eff}}(r)$ which is independent on the ion-ion correlations.⁴⁴ The Schrödinger equation that follows from this effective potential can then be solved self-consistently as described above, and the ensuing $g_{eI}(r)$ and new $C_{eI}(r)$ used to derive an effective ion-ion pair-potential from Eq. (A4), for use in the initial ion-ion loop.

*Present address: Department of Chemistry, Imperial College of Science, Technology and Medicine, Exhibition Road, London, SW7 2AY, UK.

¹Compared to the classical liquid, electron liquids are more weakly correlated [see, e.g., N.W. Ashcroft, in *Density Functional Theory*, edited by E.K.U. Gross and R. M. Dreizler (Plenum Press, New York, 1995)], which is why we refer to them as fluids instead of liquids.

²N.W. Ashcroft and D. Stroud, *Solid State Phys.* **33**, 1 (1978); R. Evans, in *Electrons in Disordered Metals and at Metal Surfaces*, Vol. 42 of *NATO Advanced Study Institute, Series B: Physics*, edited by P. Phariseau, B.L. Gyorfyy, and L. Scheire (Plenum Press, New York, 1979).

³A.A. Louis and N.W. Ashcroft, *Phys. Rev. Lett.* **81**, 4456 (1998); see also A. A. Louis and N. W. Ashcroft, *J. Non-Cryst. Solids* (to be published).

⁴S. Cusack, N.H. March, M. Parrinello, and M.P. Tosi, *J. Phys. F*

6, 749 (1976); K. Hoshino and M. Watabe, *J. Phys. Soc. Jpn.* **61**, 1663 (1992).

⁵M. Boulahbak, J.F. Wax, N. Jakse, and J.L. Bretonnet, *J. Phys.: Condens. Matter* **9**, 4017 (1997).

⁶J.F. Wax, N. Jakse, and J.L. Bretonnet, *Phys. Rev. B* **55**, 12 099 (1997).

⁷N.H. March and M. Tosi, *Laser Part. Beams* **16**, 71 (1998); N.H. March, *Curr. Sci.* **75**, 1246 (1998).

⁸S.K. Lai, K. Horii, and M. Iwamatsu, *Phys. Rev. E* **58**, 2227 (1998).

⁹A.A. Louis, Ph.D. thesis, Cornell University, 1998 (available at <http://ket.ch.cam.ac.uk/people/ardlouis/Thesis/PhDthesis.html>).

¹⁰J.A. Anta, B.J. Jesson, and P.A. Madden, *Phys. Rev. B* **58**, 6124 (1998).

¹¹W. Kohn and L.J. Sham, *Phys. Rev.* **140**, A1133 (1965).

¹²R. Car and M. Parrinello, *Phys. Rev. Lett.* **55**, 2471 (1985).

¹³G.A. de Wijs, G. Pastore, A. Selloni, and W. van der Lugt, *Phys. Rev. Lett.* **75**, 4480 (1995).

- ¹⁴M. Pearson, E. Smargiassi, and P.A. Madden, *J. Phys.: Condens. Matter* **5**, 3221 (1993).
- ¹⁵J.A. Anta and P.A. Madden, *J. Phys.: Condens. Matter* **11**, 6099 (1999).
- ¹⁶J. Chihara, *Prog. Theor. Phys.* **59**, 76 (1978).
- ¹⁷<http://xxx.lanl.gov/abs/cond-mat/9909116> (unpublished).
- ¹⁸H. Xu and J.-P. Hansen, *Phys. Rev. E* **57**, 211 (1998).
- ¹⁹N.D. Mermin, *Phys. Rev.* **137**, A1441 (1965).
- ²⁰J. Zinn-Justin, *Quantum Field Theory and Critical Phenomena* (Oxford University Press, Oxford, 1989).
- ²¹This is actually the definition of $C(\mathbf{r}, \mathbf{r}')/\beta$ (where $\beta^{-1} = k_B T$), a notation that stems from the classical context. At zero temperature, only this ratio is well defined and given by the relation (2.6); $C(\mathbf{r}, \mathbf{r}')$ itself is not.
- ²²L.S. Ornstein and F. Zernike, *Proc. R. Acad. Sci. Amsterdam* **17**, 793 (1914).
- ²³J.-P. Hansen and I. R. McDonald, *Theory of Simple Liquids, 2nd Ed.* (Academic Press, London, 1986).
- ²⁴R. Kubo, *Rep. Prog. Phys.* **19**, 255 (1966).
- ²⁵N.W. Ashcroft and N.D. Mermin, *Solid State Physics* (Holt, Rinehart and Winston, New York, 1976).
- ²⁶J. Chihara, *Prog. Theor. Phys.* **55**, 340 (1976).
- ²⁷S. Ichimaru, S. Mitake, S. Tanaka, and X-Z. Yan, *Phys. Rev. A* **32**, 1768 (1985).
- ²⁸J.K. Percus, *Phys. Rev. Lett.* **8**, 462 (1962); see also the appendix of J. Chihara, *J. Phys.: Condens. Matter* **3**, 8715 (1991).
- ²⁹Y. Rosenfeld and N.W. Ashcroft, *Phys. Rev. A* **20**, 1208 (1979).
- ³⁰J. Hafner, *From Hamiltonians to Phase Diagrams* (Springer Verlag, Berlin, 1987).
- ³¹IAMP database of [SCM-LIQ], <http://www.iamp.tohoku.ac.jp>.
- ³²G. Ortiz and P. Ballone, *Phys. Rev. B* **50**, 1391 (1994).
- ³³S. Ichimaru and K. Utsumi, *Phys. Rev. B* **24**, 7385 (1981).
- ³⁴P.A. Egelstaff, N.H. March, and N.C. McGill, *Can. J. Phys.* **52**, 1651 (1974).
- ³⁵J. Chihara, *J. Phys. F* **17**, 295 (1987).
- ³⁶H. Olbrich, H. Ruppertsberg, and S. Steeb, *Z. Naturforsch. A* **38**, 1328 (1983).
- ³⁷H. Sinn *et al.*, *Phys. Rev. Lett.* **78**, 1715 (1997).
- ³⁸S. Takeda, S. Tamaki, and Y. Waseda, *J. Phys. Soc. Jpn.* **54**, 2552 (1985) (Bi, Sn); S. Takeda, S. Harada, S. Tamaki, and Y. Waseda, *ibid.* **55**, 184 (1986) (Zn, Pb); S. Takeda *et al.*, *ibid.* **55** 3437 (1986)(Ga, Tl); **58**, 3999 (1989) (Na); **60**, 2241 (1991) (Al); **62**, 4277 (1993) (Te); **63**, 1794 (1994) (Mg); S. Takeda *et al.*, *J. Non-Cryst. Solids* **207**, 365 (1996) (Na, Mg, Al).
- ³⁹L.E. Gonzalez, D.J. Gonzalez, and K. Hoshino, *J. Phys.: Condens. Matter* **5**, 9261 (1993).
- ⁴⁰Z.W. Lu, A. Zunger, and M. Deutsch, *Phys. Rev. B* **47**, 9385 (1993).
- ⁴¹For example, small differences in standard recipes for computing resolution functions in neutron diffraction easily cause differences in the first $S_{II}(k)$ peak of order 1 to 2%, roughly equal to the effect of bonding for Li, Mg, or Al, P. Salmon private communication.
- ⁴²D.L. Price, M.L. Saboungi, and A.C. Barnes, *Phys. Rev. Lett.* **81**, 3207 (1998).
- ⁴³J. Chihara, *J. Phys. C* **18**, 3103 (1985).
- ⁴⁴J. Chihara, *Phys. Rev. A* **40**, 4507 (1989); M. Ishitobi and J. Chihara, *J. Phys.: Condens. Matter* **4**, 3679 (1992).
- ⁴⁵H. Xu, J.P. Hansen, and D. Chandler, *Europhys. Lett.* **36**, 419 (1994).
- ⁴⁶The implications of this approximation are discussed in Chap. 6 of Ref. 9.
- ⁴⁷E. Lomba, *Mol. Phys.* **68**, 87 (1989).
- ⁴⁸C. Martín, E. Lomba, J.A. Anta, and M. Lombardero, *J. Phys.: Condens. Matter* **5**, 379 (1993).
- ⁴⁹L. E. González (private communication).
- ⁵⁰J.P. Perdew and A. Zunger, *Phys. Rev. B* **23**, 5048 (1981).
- ⁵¹D.M. Ceperley and B. Alder, *Phys. Rev. Lett.* **45**, 566 (1980).
- ⁵²M.W.C. Dharma-Wardana and F. Perrot, *Phys. Rev. A* **26**, 2096 (1982).
- ⁵³L. Dagens, *J. Phys. C* **5**, 2333 (1972).
- ⁵⁴For this purpose we have modified a FORTRAN code by N. J. Troullier and J. L. Martins that solves the Kohn-Sham equation for atoms (University of Minnesota, Sept. 1989; original by S. Froyen, Berkeley).
- ⁵⁵K. Ng, *J. Chem. Phys.* **61**, 2680 (1974).